Article ID: 1000-7032(2026)04-0714-10

One-pot Microwave Hydrothermal Synthesis of Magnetic-fluorescent Carbon Dots for Latent Fingerprint Visualization

LIU Jie[1], LIU Deyang[2,3,4,5], ZHAI Chunfeng[3], GONG Qiufang[3,4], LIANG Chao[3,4*], ZHAO Yunyang[2,3,4*]

(1. *Clinical Laboratory Center, The Second Affiliated Hospital & Yuying Children's Hospital of Wenzhou Medical University, Wenzhou* 325027, *China*;
2. *Scientific Research Center, Wenzhou Medical University, Wenzhou* 325035, *China*;
3. *Cixi Biomedical Research Institute, Wenzhou Medical University, Ningbo* 315300, *China*;
4. *Institute for Advanced Research, Affiliated Cixi Hospital, Wenzhou Medical University, Ningbo* 315300, *China*;
5. *School of Information Engineering, Anhui University of Chinese Medicine, Hefei* 230012, *China*)

* *Corresponding Authors, E-mail: chaoliang@wmu. edu. cn; yunyangz@wmu. edu. cn*

Abstract: A magnetic-fluorescent nanocomposite (CDs-MNPs) was synthesized *via* a facile one-pot microwave hydrothermal method using polyethyleneimine (PEI) as a bridging agent. PEI connected magnetic nanoparticles (MNPs) and carbon dots (CDs), forming a fluffy clustered structure with nanoscale gaps, which effectively suppressed aggregation-induced photoluminescence quenching (AIQ). CDs-MNPs exhibited a saturation magnetization of 10.4 emu/g and stable solid-state green fluorescence. Benefiting from integrated magnetism, fluorescence, and strong adsorption to fingerprint residues, it achieved clear latent fingerprint (LFP) visualization on dark substrates.

Keywords: hydrothermal synthesis; magnetic-fluorescence; carbon dots; latent fingerprint
CLC number: O482. 31 **Document code**: A
DOI: 10. 37188/CJL. 20250289 **CSTR**: 32170. 14. CJL. 20250289

一步微波水热合成磁性荧光碳点用于潜在指纹可视化

刘 杰[1], 刘德洋[2,3,4,5], 翟春凤[3], 龚秋芳[3,4], 梁 超[3,4*], 赵允洋[2,3,4*]

(1. 温州医科大学附属第二医院 育英儿童医院临床检验中心, 浙江 温州 325027;
2. 温州医科大学 科研实验中心, 浙江 温州 325035;
3. 温州医科大学 慈溪生物医药研究院, 浙江 宁波 315300;
4. 温州医科大学附属慈溪医院 高等研究院, 浙江 宁波 315300;
5. 安徽中医药大学 医药信息工程学院, 安徽 合肥 230012)

摘要: 以聚乙烯亚胺(PEI)为桥接剂,通过简便的一锅法微波水热合成了一种磁性-荧光纳米复合材料(碳点磁性纳米粒子CDs-MNPs)。PEI将磁性纳米粒子(MNPs)与碳点(CDs)连接起来,形成具有纳米级间隙的蓬松簇状结构,有效抑制了聚集诱导的光致发光猝灭(AIQ)。CDs-MNPs的饱和磁化强度为10.4 emu/g,并具有稳定的固态绿色荧光。得益于其集成的磁性、荧光特性以及对指纹残留物的强吸附能力,该材料实现了深色基底上清晰的潜在指纹(LFP)显现。

关 键 词: 水热合成; 磁性-荧光; 碳点; 潜在指纹

收稿日期: 2025-12-23; **修订日期**: 2026-01-08
基金项目: 浙江省自然科学基金(LQN25C100009); 宁波市自然科学基金(2023J395); 温州医科大学人才科研启动经费(89222005)
Supported by Zhejiang Province Natural Science Foundation (LQN25C100009); Ningbo Municipal Natural Science Foundation (2023J395); Talent Scientific Research Start-up Fund of Wenzhou Medical University (89222005)

1 Introduction

Latent fingerprints (LFPs) are traces left on object surfaces by sweat, sebum, and other endogenous secretions from human fingertips. Endowed with unique ridge and furrow patterns, LFPs serve as the core basis for personal identification and play an irreplaceable role in providing direct forensic evidence in criminal investigations[1]. With the infiltration of technologies from the fields of information science and communication electronics, LFP information recognition technology has become a hot topic in interdisciplinary research, and the accurate development of LFPs in complex scenarios remains a core technical demand in this field[2].

Among various LFP development techniques, the magnetic brush method is widely used in criminal investigation practice due to its simplicity and broad applicability. Its core principle relies on the difference in adhesion between magnetic powders and LFP residues to achieve ridge visualization[2-3]. However, conventional magnetic powders with single components (*e. g.*, Fe, Al powders) adopted in traditional magnetic brush technology have significant limitations: when the detection target is on a dark or black substrate, the extremely low color contrast between the powder and the background results in blurred LFP ridges, which fails to meet the requirements for high-resolution identification[4-5]. Although single-component powders such as fluorescent particles and metal particles have been attempted to improve the development effect, how to achieve stable and efficient LFP development on diverse substrates and complex backgrounds remains an urgent technical bottleneck to be addressed.

Magnetic-fluorescent composite nanomaterials provide a new approach to break through this bottleneck: such materials not only retain the magnetism required for magnetic brush operation but also enhance the contrast with the substrate through fluorescent signals, thereby enabling clear visualization of LFPs[6]. Carbon dots (CDs), as a type of nanomaterial with excellent photoluminescent (PL) properties, are ideal candidates for constructing such composite materials[7-12]. Nevertheless, the effective combination of CDs with magnetic substrates still faces two major challenges: first, the aggregation of CDs tends to induce aggregation-induced photoluminescence quenching (AIQ); second, the strong absorption of magnetic substrates (*e. g.*, Fe_3O_4) across the entire visible light region further weakens the fluorescent signal. As a result, the preparation and application of such composite materials have rarely been reported[7-8,10].

To address the above issues, this work developed a facile one-pot microwave-assisted hydrothermal method to successfully synthesize fluorescent carbon dot-decorated magnetic nanoparticles (CDs-MNPs) and applied them to LFP development *via* the magnetic brush method as shown in Fig. 1. In the experiment, polyethyleneimine (PEI) was used as both a stabilizer and a reducing agent to promote the conversion of ammonium ferric citrate (AFC) into Fe_3O_4 magnetic nanoparticles (MNPs). Subsequently, basic fuchsin (BasF) was carbonized under microwave heating, forming green emissive CDs *in situ* on the surface of PEI-modified MNPs. Notably, the as-prepared CDs-MNPs exhibit rare solid-state green emissive properties. When applied to LFP development, this material can give full play to the dual advantages of solid-state fluorescence and magnetism, and its development effect is significantly superior to that of conventional magnetic powders. This study provides a novel synthetic strategy for the development of high-performance LFP development materials and offers more effective technical support for LFPs identification in criminal investigations.

2 Experiment

2.1 Materials

Ammonium ferric citrate (AFC) was purchased from Aladdin Scientific. Polyethylene imine (PEI) solution (average M_n ~1 800 by GPC, average M_w ~ 2 000 by LS, 50%(wt) in H_2O) was purchased from Sigma-Aldrich, Merck Ltd. Basic fuchsin (BasF) was purchased from Shanghai Macklin Biochemical Technology Co., Ltd.

2.2 Synthesis of CDs-MNPs

The synthesis of CDs-MNPs was developed from

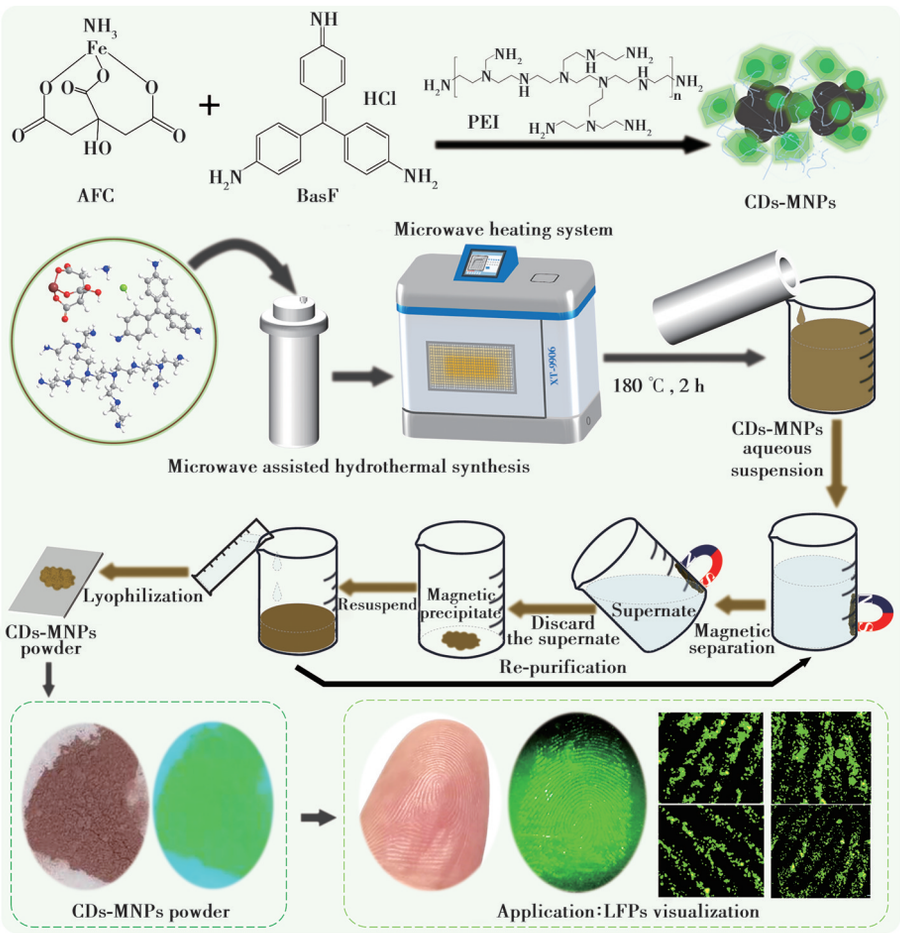

Fig.1 The synthesis process of CDs-MNPs and application for LFP extraction

the previous report[13]. Typically, AFC (1.0 g), PEI (1.0 mL) and BasF (1.0 g) were dissolved into 20 mL ultrapure water to form a homogenous solution. This solution reacted in the XT-9906 microwave oven at 180 ℃ for 2 hours, the magnetic fluorescent suspension was obtained. After purification with magnetic separations and freezing drying, the CDs-MNPs powder was finally acquired.

2.3 Characterizations

UV-Vis absorption spectra were recorded on a spectrophotometer (UV-2600, Shimadzu Corporation, Japan). The M-H curves were investigated by vibrating sample magnetometer (LakeShore7404, Lake Shore, USA). The TEM images were acquired by a Transmission Electron Microscope (JEM-F200, JEOL, Japan) operating at 200 kV. The magnetic samples were prepared by being dispersed in water/ethanol, then dropped on an opened double copper grid with carbon film and dried under an infrared baking lamp and closed it. Elemental analysis was carried out *via* energy-dispersive X-ray spectroscopy (EDS) mapping, using an Oxford instrument attached to the TEM. SEM images were obtained on scanning electron microscopy (SU8600, Hitachi, Japan). XRD pattern was performed on X-ray diffractometer (Smartlab, Rigaku, USA). The excitation emission maps were also obtained on the FS5 fluorescence spectrophotometer (FS5, Edinburgh instruments Ltd., UK) by using a Xe lamp as an excitation source with the excitation wavelength step of 5 nm. The used holder was SC-20 sample module with cuvette holder under room temperature. FTIR spectra were tested on Fourier Transform Infrared Spectrometer (NICOLET is20, Thermo, USA). XPS spectra were carried out on an X-ray photoelectron spectroscopy (ESCALAB 250Xi, Thermo Fisher Scientific, USA) at 12.5 kV under the pressure of 8×10^{-10} Pa. The binding energy of C 1s at 284.60 eV is used as the energy reference to correct the charge.

3　Results and Discussion

In this work, the solid-state emissive CDs-MNPs were synthesized by one-pot microwave-hydrothermal method[13]. The excitation-emission maps (EEMs) of CDs-MNPs in powder, aqueous and ethanol suspension in Fig. 2(a)-(c) showed that CDs-MNPs have a green emission not only in powder but also in aqueous and ethanol suspension. Besides the solid-state green emission, the CDs-MNPs also exhibit red emission due to the fluorescence resonance energy transfer (FRET) in powder which makes the moderate distance among different CDs to prevent the AIQ. Due to the short wavelength emissive cross-linked chain polymers in CDs-MNPs were dissolved in water, the FRET among different fluorophores was eliminated, which leads to the excitation-independent PL property of CDs-MNPs in water. Comparing to the CDs-MNPs in H_2O, CDs-MNPs in ethanol have a few more emission center like blue-purple emission, suggesting water can extend the distance among these particles in CDs-MNPs to eliminate the FRET thoroughly. This could be explained by Scheme S1 in the supporting information. The CDs-MNPs from powder state to ethanol and aqueous suspension, the FRET was eliminated gradually due to the increased dispersibility.

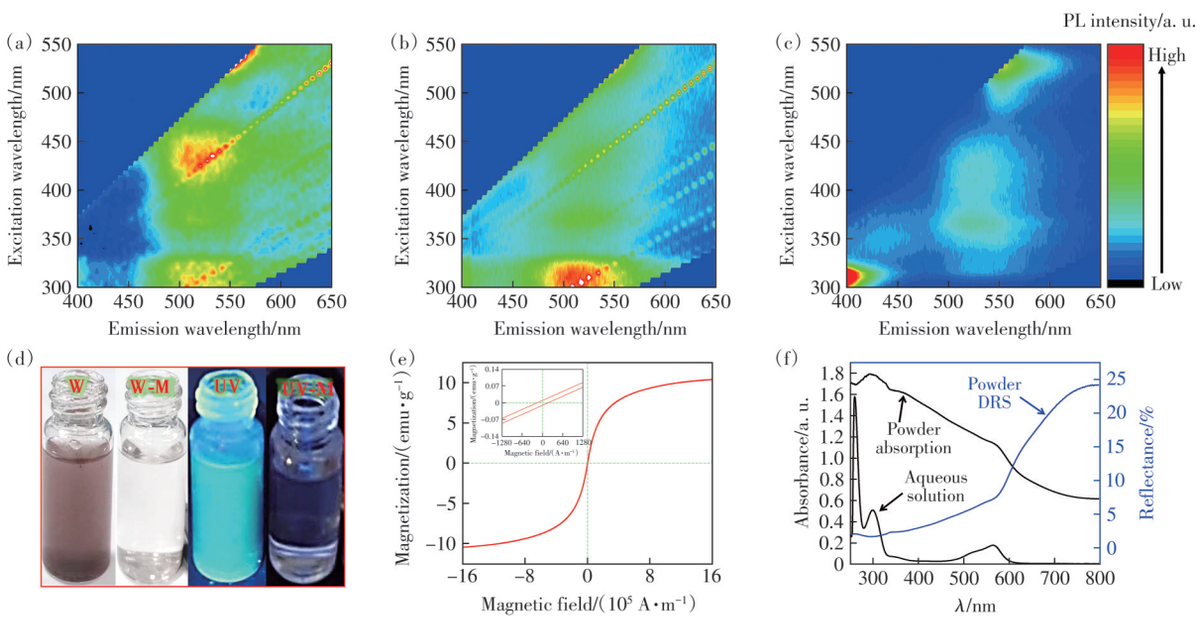

Fig.2　EEMs of CDs-MNPs in (a) powder, (b) water, and (c) ethanol. (d) Photographs of CDs-MNPs under daylight (W) and 365 nm UV light (UV) without/with a magnetic field (M, applied on the right). "W", "UV", and "M" denote images acquired under white light, 365 nm UV light, and with a right-sided magnetic field, respectively. (e) Room-temperature M-H loops of CDs-MNPs (inset: enlarged M-H curves). (f) Absorption spectra of CDs-MNPs (powder and aqueous solution) and powder DRS of CDs-MNPs

Fig. 2(d) presents the optical images of CDs-MNPs under daylight and ultraviolet (UV) light (365 nm), with and without an external magnetic field (applied to the right side of the vial). It can be clearly observed that CDs-MNPs aggregate entirely on the right side of the vial upon exposure to the magnetic field, confirming their magnetic responsiveness. Additionally, the CDs-MNPs suspension emits cyan-green fluorescence under UV light, while the solid powder exhibits green fluorescence (Fig. 1). These macroscopic phenomena directly confirm the successful synthesis of the magnetic-fluorescent CDs-MNPs composite. The magnetic properties of CDs-MNPs were characterized using a vibrating sample magnetometer (VSM). As shown in Fig. 2(e), the saturation magnetization (M_s) value of CDs-MNPs is 10.4 emu/g. The inset of Fig. 2(e) displays the enlarged magnetization-hysteresis (M—H) loops, which reveal a slight hysteresis effect with a coercive force (H_c) of 328 A/m(4.1 Oe). This observation indicates that CDs act as magnetic domain walls within the CDs-MNPs composite, leading to an

irreversible magnetization process. Collectively, these results demonstrate the paramagnetic behavior of CDs-MNPs, further verifying the successful preparation of the magnetic-fluorescent material. Fig. 2(f) shows the absorption spectra of CDs-MNPs in aqueous solution and powder form, as well as the powder diffuse reflectance spectrum (DRS). As evident from the spectra, CDs-MNPs exhibit strong absorption in the UV region and an additional absorption band at ~ 570 nm (followed by a rapid decrease in absorbance) regardless of their state (powder or aqueous solution). This absorption feature is characteristic of CDs, thus confirming the successful formation of CDs in the composite. Furthermore, the significant diffuse reflectance in the red and near-infrared (NIR) regions is attributed to the MNPs component.

The microstructure of CDs-MNPs was systematically characterized by transmission electron microscopy (TEM), high-resolution TEM (HRTEM), and scanning electron microscopy (SEM) as shown in Fig. 3. In TEM image, the CDs-MNPs exhibit a nanoscale clustered structure. HRTEM image reveals that the CDs-MNPs are composed of graphitized CDs and crystalline Fe_3O_4 (Fig. 3(a) and Fig. S2). The crystalline structure with observed lattice spacing of 0.21, 0.24 nm related to the (1 0 0) plane and (1 1 2 0) in-plane lattice spacing of graphite was clearly identified, indicating the crystalline graphene-like core of CDs in CDs-MNPs[14-16]. The lattice spacing of 0.29 nm was attributed to the (2 2 0) lattice planes of the cubic Fe_3O_4, which corresponds to the diffraction peak at the 2θ=31° in XRD (Fig. 4(a)), respectively[17-18]. These nanoparticles are typically crosslinked through amorphous structures to form stable clusters, which is similar to the previous work[19]. Selected area electron diffraction (SAED) patterns display diffraction rings corresponding to different crystal phases, including the (3 1 1) and (4 0 0) lattice planes of Fe_3O_4, as well as an extremely weak diffraction ring assigned to the (0 0 2) lattice plane of the graphitic structure of CDs—attributed to the strong background signal from the carbon film. Energy-dispersive X-ray spectroscopy (EDS) elemental mapping (Fig. 3(b)) shows that

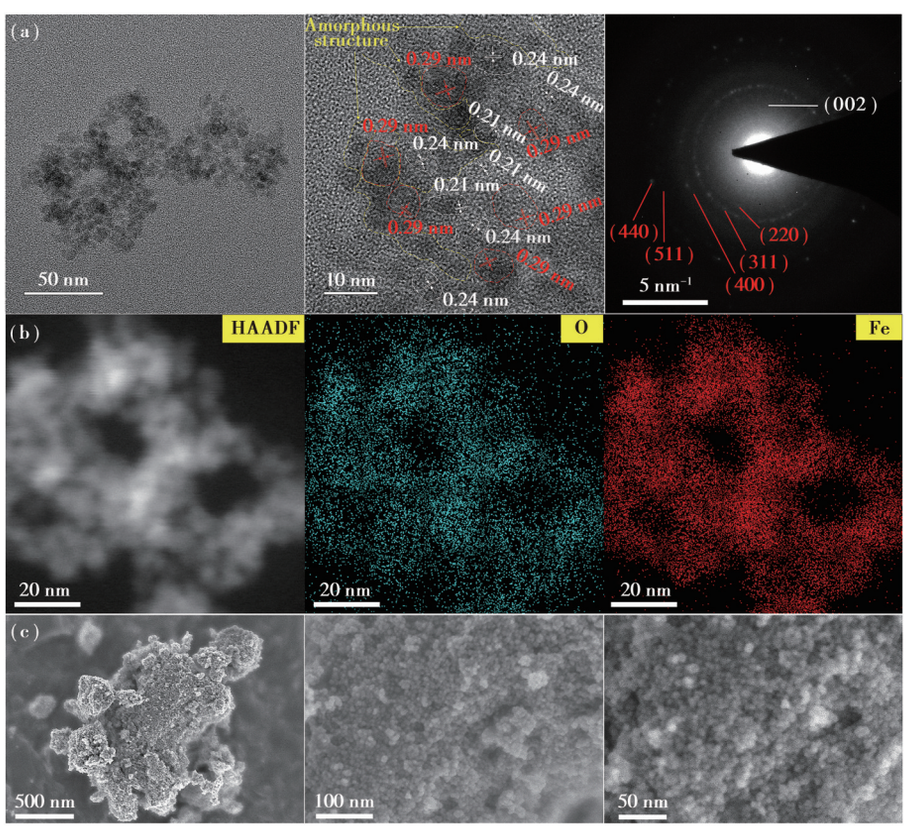

Fig.3 (a) TEM (left), HRTEM (middle, enlarged image), SAED pattern (right) of CDs-MNPs. (b) EDS mapping and (c) SEM imaging of CDs-MNPs with different magnifications

the distribution of O does not fully overlap with that of Fe. This observation indicates the presence of oxygen atoms from CDs in addition to the background contribution from the carbon film, thereby confirming the relatively uniform crosslinking between CDs and MNPs. Such uniform crosslinking is proposed to be one of the key factors enabling the solid-state emission of CDs-MNPs. Scanning electron microscopy (SEM) images of the composite powder at different magnifications (Fig. 3(c)) reveal a fluffy surface morphology, with bright light-gray particles well-separated from each other. The fluffy morphology of CDs-MNPs with nanoscale gaps directly confirms the absence of AIQ. This structural feature not only facilitates light penetration but also provides a favorable microstructural basis for the solid-state emission of CDs-MNPs.

The X-ray diffraction (XRD) was employed to determine CDs-MNPs crystal structure as shown in Fig. 4(a). The diffraction peaks at 31°, 36°, 43.5°, 54°, 58°, 63.5° correspond to the (2 2 0), (3 1 1), (4 0 0), (4 2 2), (5 1 1), (4 4 0) plane showed the formation of Fe_3O_4 MNPs[17, 20]. The new sharp diffraction peak arose in CDs-MNPs indicating CDs formed the new crystal structures on the surface of MNPs. The emergence of new sharp diffraction peaks (2θ=9°~28°) in the XRD pattern of CDs-MNPs indicates that CDs facilitate the formation of new crystals, which may act as a matrix for solid-state emission. The chemical structure of CDs-MNPs was also characterized *via* Fourier transform infrared (FTIR) spectrum. As shown in Fig. 4(b), characteristic absorption bands assigned to the bending and stretching vibrations of C—H (750–1 000 cm^{-1} and 3 010 cm^{-1}) and C═C (1 623/1 503 cm^{-1}) bonds in aromatic moieties were observed. These bands confirm the presence of sp^2 C domains, thus verifying the successful formation of CDs in CDs-MNPs. Additionally, a distinct absorption peak at 1 146 cm^{-1}, corresponding to the stretching vibration of C—N bonds, indicates that CDs are covalently linked to MNPs *via* C—N bridges in the CDs-MNPs architecture. These characteristic structures also endow the CDs-MNPs with the potential for adsorbing fingerprint residues. The abundant organic functional groups on the surface of CDs-MNPs can form strong interactions (*e. g.*, hydrogen bonds and van der Waals forces) with fingerprint residues based on the principle of like-dissolves-like, which provides a structural basis for efficient LFP extraction.

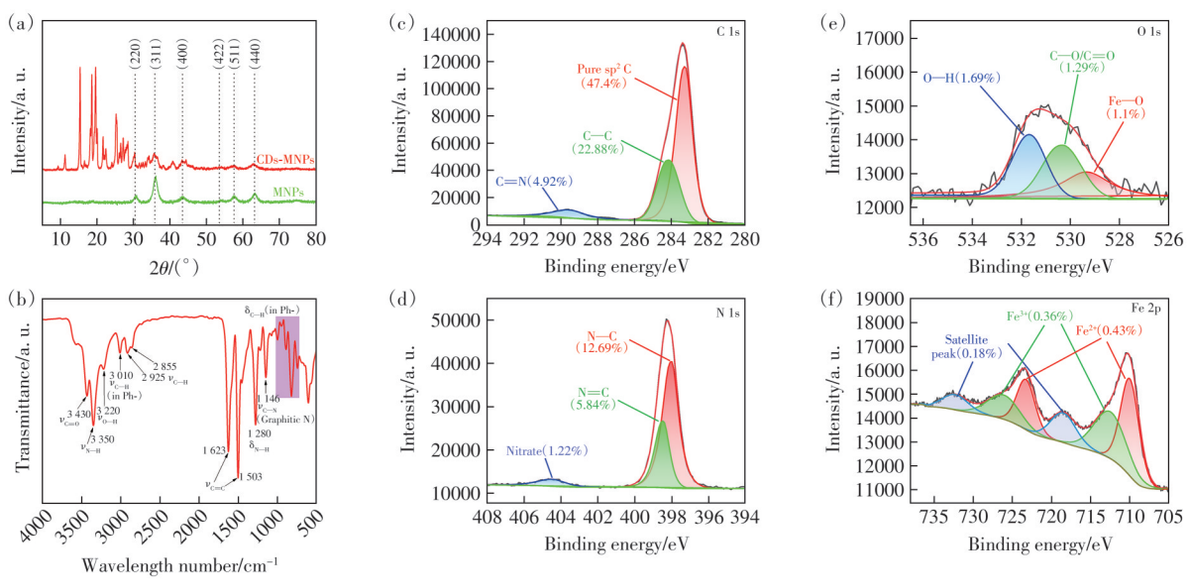

Fig.4　The XRD pattern (a), FTIR (b), and high-resolution XPS of C 1s (c), N 1s (d), O 1s (e), and Fe 2p (f) spectra of CDs-MNPs

In order to further analyze the special structure of CDs-MNPs, X-ray photoelectron spectroscopy (XPS) was carried out to characterize the chemical valence of the CDs-MNPs, showed in Fig. 4(c)–(f).

In the C 1s spectra, it showed that CDs-MNPs had a high content of conjugated sp^2 carbon, suggesting the formation of CDs graphitic structure. CDs-MNPs sample had over 75 % of C, which confirms the high ratio of CDs in CDs-MNPs sample. The high resolution XPS of O 1s and Fe 2p spectra showed CDs-MNPs had the contents of Fe^{3+} (0.36%) and Fe^{2+} (0.43 %) and Fe—O (1.1%), indicating the formation of MNPs. The content ratio of Fe to Fe—O was essentially consistent with the stoichiometric ratio of MNPs. Nevertheless, the experimentally determined Fe^{2+}/Fe^{3+} ratio deviated from the theoretical value (1∶2), which was presumably attributed to the organic crosslinking interaction between MNPs and CDs mediated by amorphous components (*e. g.*, PEI fragment) within CDs-MNPs. In addition, the peak at a binding energy of 404.6 eV is assigned to nitrate species in N 1s spectra, indicating the possible presence of trace amounts of ferrous nitrate in CDs-MNPs composite (Fig. 4(d)).

The PL mechanism of CDs is closely correlated with their intricate chemical structure. Most CDs lack solid-state PL properties due to the typical AIQ effect, and this limitation is exacerbated in CDs with MNPs composites by the strong visible-light absorption of Fe_3O_4. As illustrated in Schematic S1, the structural architecture of CDs-MNPs can be elucidated as follows: PEI chains bridge MNPs and CDs, maintaining an optimal interparticle distance and constructing a fluffy clustered structure. This spatial separation not only mitigates PL quenching of CDs by Fe_3O_4 but also enables FRET between CDs, while simultaneously suppressing AIQ to achieve solid-state emission. When dispersed in water, CDs are slightly detached from Fe_3O_4; although the CD-Fe_3O_4 distance is marginally increased, FRET persists, resulting in weak blue-purple emission and intense green emission. In contrast, the excellent dispersibility of CDs-MNPs in ethanol thoroughly enlarges the interparticle distance, eliminating FRET and thereby yielding strong blue-purple emission (from amorphous components) with attenuated excitation-independent green emission (from graphitic components)[21].

Benefiting from their excellent solid-state emission and magnetic responsiveness, coupled with the presence of nanoscale voids among particles that facilitate the adsorption of fingerprint residues (Fig. 3(c)), CDs-MNPs were applied for LFPs extraction. The process of applying this powder for LFPs extraction *via* the magnetic brush method is illustrated in Fig. 5(a). The fluorescent images of the LFPs developed with CDs-MNPs powder on the glass and ceramic sheet substrates demonstrate the application potential of the CDs-MNPs for LFPs extraction on diverse substrates as shown in Fig. 5(b) and Fig. S3. As a powerful artificial intelligence (AI) tool, Python-assisted digital processing has emerged as an essential approach for LFPs image analysis (Fig. 5(b)). This method relies on minutiae features extracted from intrinsic local information points of fingerprint images *via* computer algorithms. Effective feature extraction requires the original LFPs image to possess distinct Level 1 and Level 2 structural features. Prior to feature point extraction, the original fluorescent LFP image is converted into a binary format through three sequential steps as showed in Fig. 5(b): (1) transforming the input color image into a grayscale image; (2) normalizing the grayscale image to enhance the target outline; and (3) performing binarization by classifying pixels into two categories ("1" for white and "0" for black) based on their grayscale values. This not only sharply highlights the contour of LFP ridges but also lays a critical foundation for subsequent computer-aided minutiae extraction (*e. g.*, termination, bifurcation, core) and quantitative analysis. Collectively, this image processing workflow significantly improves the signal-to-noise ratio of LFP images, ensuring the reliability and accuracy of LFP feature recognition, thereby facilitating the practical application of CDs-MNPs in forensic identification. All the minutia points representing important features of LFPs on a black substrate were clearly observed by confocal fluorescent microscopy in Fig. 5(c) and Fig. S3(c), including terminations, whorl cores, bifurcations, short ridges, deltas, ridge divergences, and crossovers, respectively. These distinct feature points were easily identified, indicating the great potential

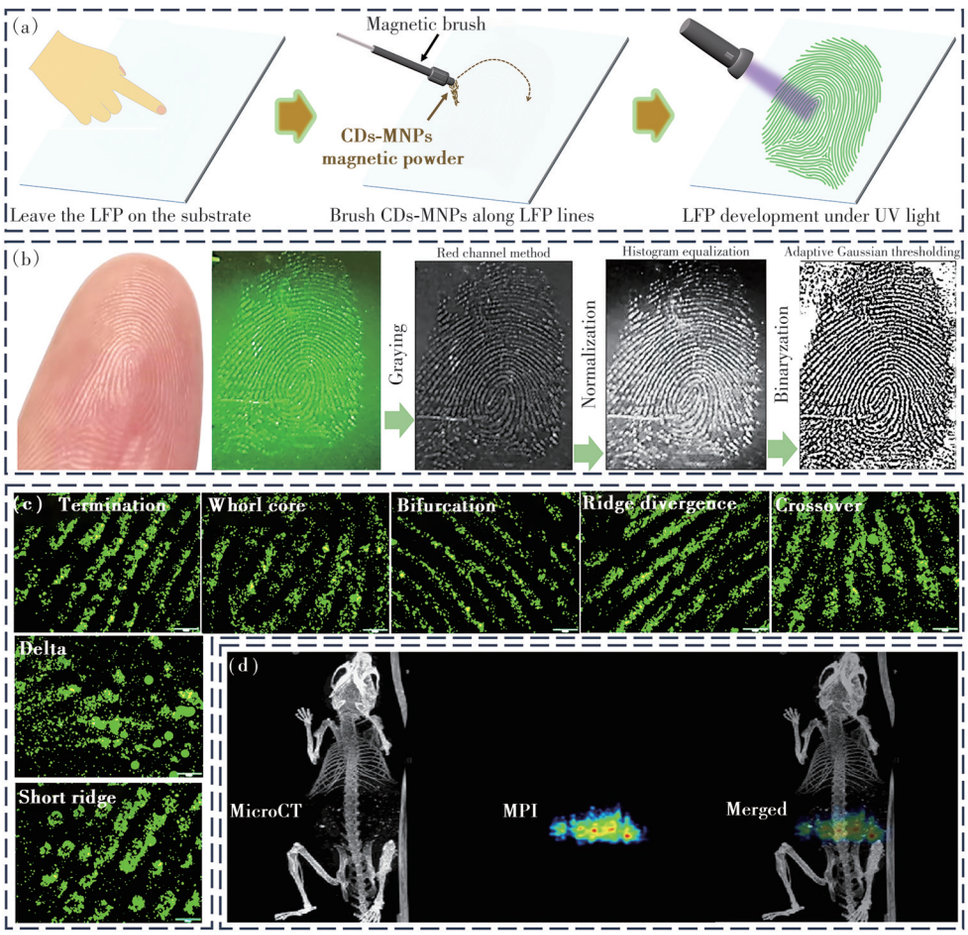

Fig.5　(a) The LFPs extraction process with CDs-MNPs *via* magnetic brush method. (b) The picture of the volunteer's finger, the corresponding fluorescent LFPs image on the glass substrate under UV light on black stained by CDs-MNPs powder, and the binarization process of fluorescent LFPs image. (c) The confocal fluorescence images showing 7 kinds of character details: (1) termination, (2) whorl core, (3) bifurcation, (4) ridge divergence, (5) crossover, (6) delta, and (7) short ridge. (d) The biodistribution of CDs-MNPs intragastrically administered was monitored *via* Micro-CT and MPI

of CDs-MNPs powder for LFPs extraction. In addition, this work explored the potential application of CDs-MNPs in biological imaging. As shown in Fig. 5(d), the micro-computed tomography (Micro-CT) and magnetic particle imaging (MPI) of healthy mice after intragastric administration demonstrate that CDs-MNPs hold great potential as an MPI contrast agent *in vivo* lesion visualization[22].

4　Conclusion

In summary, we developed a facile one-pot microwave hydrothermal method for synthesizing magnetic fluorescent CDs-MNPs nanocomposites. PEI served as a bridging agent to connect MNPs and CDs, constructing a fluffy clustered structure with nanoscale gaps between particles. This unique architecture not only effectively suppresses AIQ of CDs in the powder state to enable stable solid-state emission but also facilitates the adsorption of fingerprint residues. Benefiting from its integrated magnetic responsiveness and solid-state emission properties, the CDs-MNPs powder exhibits distinct advantages for LFP extraction *via* the magnetic brush method on dark substrates. Notably, this work addresses the technical gap in LFP extraction on dark backgrounds and provides a novel strategy for the synthesis of multi-functional composite materials with synergistic performance.

Supplementary Information and Response Letter are available for this paper at: http://cjl.lightpublishing.cn/thesisDetails#10.37188/CJL.20250289

References:

[1] LIANG M W, DU B, WANG J, *et al*. A strategy for the simultaneous visualization of latent fingerprints and touch DNA based on fluorescent functional metal-organic framework sensing platform [J]. *Sens. Actuators* B *Chem.*, 2025, 444: 138479.

[2] YOON J H, JIN Y J, SAKAGUCHI T, *et al*. Visualization of sweat fingerprints on various surfaces using a conjugated polyelectrolyte [J]. *ACS Appl. Mater. Interfaces*, 2016, 8(36): 24025-24029.

[3] LIU L, ZHOU H, CHEN H Y, *et al*. Particle size-tunable polydopamine nanoparticles for optical and electrochemical imaging of latent fingerprints on various surfaces [J]. *ACS Appl. Mater. Interfaces*, 2024, 16(28): 37265-37274.

[4] WAN J W, CHEN L, LI W, *et al*. Preparation of novel magnetic nanomaterials based on "facile coprecipitation" for developing latent fingerprints (LFP) in crime scenes [J]. *ACS Omega*, 2022, 7(2): 1712-1721.

[5] TIAN L, CHEN H Y, SUN X Y, *et al*. Wet nitrocellulose membrane for the level 3 feature visualization of various latent fingerprints and gender determination [J]. *Analyst*, 2023, 148(11): 2438-2448.

[6] TAMBOLI S, NAIR G B, KROON R E, *et al*. High-contrast multi-surface imaging of latent fingerprints using color-tunable YOF: Tb^{3+}, Eu^{3+} ultrafine nanophosphors with high quantum yield [J]. *Dalton Trans.*, 2024, 53(28): 11736-11749.

[7] DONG X Y, NIU X Q, ZHANG Z Y, *et al*. Red fluorescent carbon dot powder for accurate latent fingerprint identification using an artificial intelligence program [J]. *ACS Appl. Mater. Interfaces*, 2020, 12(26): 29549-29555.

[8] NIU X Q, SONG T B, XIONG H M. Large scale synthesis of red emissive carbon dots powder by solid state reaction for fingerprint identification [J]. *Chin. Chem. Lett.*, 2021, 32(6): 1953-1956.

[9] ZHAO Y Y, ZUO S L, MIAO M. The effect of oxygen on the microwave-assisted synthesis of carbon quantum dots from polyethylene glycol [J]. *RSC Adv.*, 2017, 7(27): 16637-16643.

[10] YU B J, LIU S D, XIE W H, *et al*. Versatile core-shell magnetic fluorescent mesoporous microspheres for multilevel latent fingerprints magneto-optic information recognition [J]. *InfoMat*, 2022, 4(5): e12289.

[11] 张路鹏, 张清梅, 何松杰, 等. 碳点的功能化研究进展 [J]. 发光学报, 2022, 43(7): 1147-1163.
ZHANG L P, ZHANG Q M, HE S J, *et al*. Progress on functionalization of carbon dots [J]. *Chin. J. Lumin.*, 2022, 43(7): 1147-1163. (in Chinese)

[12] 张震, 曲丹, 安丽, 等. 荧光碳点的制备、发光机理及应用 [J]. 发光学报, 2021, 42(8): 1125-1140.
ZHANG Z, QU D, AN L, *et al*. Preparation, luminescence mechanism and application of fluorescent carbon dots [J]. *Chin. J. Lumin.*, 2021, 42(8): 1125-1140. (in Chinese)

[13] ZHAO Y Y, LIU J, LIU D Y, *et al*. Magnetic fluorescent carbon dots synthesized *via* one-pot approach for tumor photothermal therapy [J]. *iScience*, 2026, 29(1): 114366.

[14] ZHANG Q, WANG R Y, FENG B W, *et al*. Photoluminescence mechanism of carbon dots: triggering high-color-purity red fluorescence emission through edge amino protonation [J]. *Nat. Commun.*, 2021, 12(1): 6856.

[15] PARK H, PARK S Y. Enhancing the alkaline hydrogen evolution reaction of graphene quantum dots by ethylenediamine functionalization [J]. *ACS Appl. Mater. Interfaces*, 2022, 14(23): 26733-26741.

[16] WANG L M, WANG B Z, LIU E S, *et al*. Polyetherimide functionalized carbon dots with enhanced red emission in aqueous solution for bioimaging [J]. *Chin. Chem. Lett.*, 2022, 33(8): 4111-4115.

[17] ZHANG T T, WANG Z J, XIANG H J, *et al*. Biocompatible superparamagnetic europium-doped iron oxide nanoparticle clusters as multifunctional nanoprobes for multimodal *in vivo* imaging [J]. *ACS Appl. Mater. Interfaces*, 2021, 13(29): 33850-33861.

[18] BOUDOUH D, HAMANA D, METSELAAR H S C, *et al*. Low-temperature green route synthesis of Fe_3O_4—C nanocomposite using Olive Leaves Extract [J]. *Mater. Sci. Eng.* B, 2021, 271: 115276.

[19] ZHAO Y Y, QU S N, FENG X Y, *et al*. Tailoring the photoluminescence excitation dependence of the carbon dots *via* an alkali treatment [J]. *J. Phys. Chem. Lett.*, 2019, 10(16): 4596-4602.

[20] XIE R Y, QU Y Y, TANG M Y, *et al*. Carbon dots-magnetic nanocomposites for the detection and removal of Hg^{2+} [J]. *Food Chem.*, 2021, 364: 130366.

[21] ZHAO Y Y, HE B C, LIU E S, *et al*. Aluminum-based surface polymerization on carbon dots with aggregation-enhanced luminescence [J]. *J. Phys. Chem. Lett.*, 2021, 12(19): 4530-4536.

[22] 姜欣雨, 杨柏. 药物碳点的分类、性质及生物医用[J]. 发光学报, 2025, 46(5): 813-829.
JIANG X Y, YANG B. Classification, properties and biomedical applications of pharmaceutical carbon dots [J]. *Chin. J. Lumin.*, 2025, 46(5): 813-829. (in Chinese)

刘杰(1996-),女,安徽六安人,学士,2020年于蚌埠医学院获得学士学位,主要从事生物材料应用的研究。
E-mail: 1948506659@qq.com

赵允洋(1988-),男,安徽亳州人,博士,助理研究员,2021年于中国澳门大学获得博士学位,主要从事荧光碳点合成与应用的研究。
E-mail: yunyangz@wmu.edu.cn

梁超(1991-),男,安徽芜湖人,博士,研究员,2019年于苏州大学获得博士学位,主要从事生物纳米材料用于肿瘤治疗、抑制肿瘤转移与改善肿瘤微环境的研究。
E-mail: liangchao@wmu.edu.cn